This is a repository copy of *Facile one-pot synthesis of dual-cation incorporated titanosilicate and its deposition to membrane surfaces for simultaneous removal of Cs^+ and Sr^{2+}*.

Article:

Kim, YK, Kim, S, Kim, Y et al. (3 more authors) (2019) Facile one-pot synthesis of dual-cation incorporated titanosilicate and its deposition to membrane surfaces for simultaneous removal of Cs^+ and Sr^{2+}. Applied Surface Science, 493. pp. 165-176. ISSN 0169-4332

https://doi.org/10.1016/j.apsusc.2019.07.008

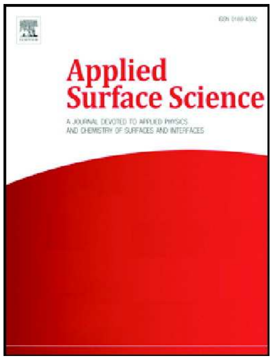

Facile one-pot synthesis of dual-cation incorporated titanosilicate and its deposition to membrane surfaces for simultaneous removal of Cs+ and Sr2+

Yun Kon Kim, Sungjun Kim, Yonghwan Kim, Kyeonghui Bae, David Harbottle, Jae W. Lee

PII: S0169-4332(19)32044-6
DOI: https://doi.org/10.1016/j.apsusc.2019.07.008
Reference: APSUSC 43266

To appear in: *Applied Surface Science*

Received date: 26 March 2019
Revised date: 17 June 2019
Accepted date: 1 July 2019

Please cite this article as: Y.K. Kim, S. Kim, Y. Kim, et al., Facile one-pot synthesis of dual-cation incorporated titanosilicate and its deposition to membrane surfaces for simultaneous removal of Cs+ and Sr2+, Applied Surface Science, https://doi.org/10.1016/j.apsusc.2019.07.008

Facile one-pot synthesis of dual-cation incorporated titanosilicate and its deposition to membrane surfaces for simultaneous removal of Cs^+ and Sr^{2+}

Yun Kon Kim[a], Sungjun Kim[a], Yonghwan Kim[a], Kyeonghui Bae[a], David Harbottle[b] and Jae W. Lee [a],*

[a]Department of Chemical and Biomolecular Engineering, Korea Advanced Institute of Science and Technology (KAIST), Daejeon 305-701, Republic of Korea

[b]School of Chemical and Process Engineering, University of Leeds, Leeds LS2 9JT, United Kingdom

*Corresponding author. Tel: +82-42-350-3940. E-mail: jaewlee@kaist.ac.kr

KEYWORDS: Cesium, Strontium, Titanosilicate, Ion exchange, Membrane

Abstract

Selective removal of ^{137}Cs and ^{90}Sr from aqueous environments is essential for the volume reduction and ultimate safe storage of nuclear waste. This study introduces a facile one-pot hydrothermal synthesis of Dual-cation form of TitanoSilicate (DTS, $M_3HTi_4O_4(SiO_4)_3$, M = Na^+ and K^+) for the effective and simultaneous removal of Cs^+ and Sr^{2+}. DTS showed enhanced adsorption capacities (469 mg/g for Cs^+ and 179 mg/g for Sr^{2+}) and the adsorption kinetics were extremely fast with around 98 % and greater than 99 % removal achieved within 1 min from a dilute Cs^+ and Sr^{2+} solution, respectively. Moreover, DTS indicated the superior selectivity for both Cs^+ and Sr^{2+} due to the dual-cation incorporation in the structure. In groundwater, the distribution coefficients (K_d at V/m = 1000 mL/g) for DTS were high for both Cs^+ (1 ppm, 2.9×10^5 mL/g) and Sr^{2+} (1 ppm, 1.0×10^5 mL/g), and even in seawater DTS maintained a Cs^+ (1 ppm) K_d value as high as 4.9×10^4 mL/g. Remarkably, DTS is synthesized as a membrane with graphene oxide for continuous removal of the radionuclides, which is extremely beneficial to purifying a large volume of contaminated water.

Introduction

Nuclear power is considered a sustainable and efficient carbon free energy source [1]. However, there remains ongoing societal concerns due to the potential emission of radioactive waste, approximately 2000 - 2300 metric tons of high-level radioactive waste per year in the United States [2, 3]. Radionuclides in effluents must be separated, treated, and stored safely to prevent any detrimental effect to the environment [4, 5]. Among them, ^{137}Cs, ^{134}Cs and ^{90}Sr are the most hazardous radionuclides due to the emission of gamma-rays and high energy beta particles, respectively, and the high probability of production during the nuclear fission process [6-8]. In particular, ^{137}Cs and ^{90}Sr have half-lives of approximately 30 years, indicating long-lasting radioactivity after about several centuries [9-12]. However, removal of these radionuclides from environmental systems has been rather challenging since the radionuclides are present in very low concentrations (ppm level or below) and coexist with a large excess of competing cations (Na^+, K^+, Mg^{2+}, Ca^{2+} and others) [13-15]. Several different methods have been demonstrated for the separation of radioactive Cs and Sr such as liquid-liquid extraction, chemical precipitation, evaporation, and ion exchange, which are also traditional methods for wastewater treatment [16-19]. Among them, ion exchange is an efficient process for the recovery of radionuclides from aqueous nuclear wastes due to its convenient, selective, and high capacitive properties, resulting in a minimum solidified waste [20-22].

Among various ion exchange materials such as zeolites [23], clay minerals [21, 24, 25], and chalcogenide [1, 26], titanosilicates are exceptionally good candidates that meet the required material properties of chemical and radiation stability, high selectivity, and high sorption capacity over a broad pH range [27-29]. Two types of titanosilicates with chemical compositions of $Na_2Ti_2O_3SiO_4$•$2H_2O$ and $M_3HTi_4O_4(SiO_4)_3$•$4H_2O$ (M = alkali metal) have attracted considerable interest as adsorbents for the removal of radioactive Cs^+ and Sr^{2+} ions [30, 31]. The former is called crystalline titanosilicate material (CST), whose proton-exchanged form (H-CST) exhibits remarkable Cs^+ selectivity even in a highly concentrated sodium solution, but poor removal efficiency for Sr^{2+} [10]. The latter is a synthetic analogue of mineral pharmacosiderite ($KFe_4(OH)_5(AsO_4)_3$) [32]. This titanosilicate compound has a three dimensional structure by 8-membered ring windows, which are composed of face-sharing TiO_6 octahedral units (formation of cubane-like Ti_4O_4 unit), and vertices-sharing SiO_4 tetrahedral units [33]. The charge-balancing extra framework cations occupy the 8-membered windows and are coordinated by the surrounding oxygens. Previous studies have revealed that the pharmacosiderite type titanosilicate is effective for the removal of Cs^+ and Sr^{2+} in the presence of ppm level of competing cations [34]. However, the material performance highly depends on the types of extra framework cations such as Na^+ and K^+, and hence the multi-step preparation and additional ion exchange are required to induce different types of cation forms according to the targeting ions, which limit its practical application to large scale processes in order to achieve effective simultaneous removal of Cs^+ and Sr^{2+} [30, 34, 35].

Here, we introduced a facile one-pot synthesis of a **D**ual-cation (Na^+ & K^+) incorporated pharmacosiderite type **T**itano**S**ilicate (DTS). The design mechanism is to directly induce the dual-cation phase through the exchange of cations between K^+ and Na^+ with formation of the pharmacosiderite type titanosilicate in a one-pot route to obtain an effective ion exchanger for both Cs^+ and Sr^{2+}. The topotactic ion exchange process of dual cations with Cs^+ and Sr^{2+} was studied using various spectroscopic analysis techniques. Interestingly, compared to the previously reported K^+ and Na^+ forms of titanosilicates [34], DTS exhibits not only higher adsorption capacity, but enhanced selectivity for the simultaneous removal of Cs^+ and Sr^{2+}, which facilitates more practical utilization following a simplified preparation procedure. Moreover, we demonstrated that DTS retains a very high distribution coefficient (K_d, mL/g) for the immobilization of Cs^+ and Sr^{2+} with rapid removal kinetics and remains stable over a wide pH range. In particular, DTS remains highly effective for the simultaneous removal of Cs^+ and Sr^{2+} ions when immersed in an aqueous solution containing various competing cations. Practically, this study also demonstrated a possible application of DTS as active sites in a composite membrane with graphene oxide (GO) for continuous separation of Cs^+ and Sr^{2+}.

Experimental Section

Materials

All chemicals were used as received without further purification. Sodium silicate ($Na_2O(SiO_2)_x$•xH_2O), fumed silica, titanium (III) chloride (12 wt% $TiCl_3$ in hydrochloric acid), potassium fluoride, strontium chloride hexahydrate, graphite powder and untreated seawater (S9148) were purchased from Sigma-Aldrich. Titanium (IV) isopropoxide, sodium hydroxide, and hydrochloric acid were supplied by JUNSEI Chemical. Cesium chloride was purchased from Alfa Aesar, and potassium hydroxide was obtained from DAEJUNG Co., Ltd. Polyethersulfone membrane (PES, 47 mm, 0.22 μm) was supplied by Millipore.

Synthesis of Dual-cation (Na^+ and K^+) incorporated TitanoSilicate (DTS)

The pharmacosiderite type titanosilicate containing both Na^+ and K^+ (DTS) was synthesized via a simple one-step hydrothermal route. Typically, NaOH (9 g), KOH (4.5 g), KF (4.7 g), sodium silicate (11 g), $TiCl_3$ (12.8 g), and DI water (54 g) were mixed and vigorously stirred at 30 °C for 2 h. The mixture was then transferred into a 100 mL Teflon-lined autoclave, sealed, and heated in an oven at 180 °C for 4 days. The product was collected by vacuum filtration and thoroughly washed with DI water and ethanol in sequence. Finally, the DTS was dried overnight in an oven at 80 °C.

Synthesis of GO and DTS membrane (GDM)

The GO and DTS membrane (GDM) was prepared using a vacuum-assisted filtration method. Typically, the synthesized GO powder (80 mg) was dispersed in 1000 mL of DI water, and continuously sonicated for 10 h. The GO suspension was centrifuged with 5000 rpm for 1h, and the supernatant was recovered. The dilute GO suspension was filtered on a PES membrane under a moderate vacuum condition. After that, 1 mg/mL of DTS (40 mg in 40 mL DI water) was poured on the pre-formed GO layer and vacuum-filtered. Finally, the synthesized GDM was dried in an oven at 30 °C overnight.

Ion exchange experiments

Initial and specific Cs^+ and Sr^{2+} ion concentrations were quantified in triplicate using inductively coupled plasma mass spectroscopy (ICP-MS 7700S, Agilent) and the average value was reported. Unless otherwise noted, the solution volume (mL) to ion exchanger mass ratio (g) is 1000 mL/g. The adsorption capacity (q_e, mg/g), removal efficiency (RE, %), and distribution coefficient (K_d, mL/g) were calculated by equation (1), (2), and (3):

$$q_e = \frac{(C_0 - C_f)V}{m} \qquad (1)$$

$$K_d = \frac{(C_0 - C_f)}{C_f}\frac{V}{m} \qquad (2)$$

$$RE = \frac{(C_0 - C_f)}{C_0} \times 100 \qquad (3)$$

In Eqs. 1, 2, and 3, C_0 and C_f are the initial and final ion concentrations (mg/L) as measured by ICP-MS. V and m represent the total volume of solution (L or mL) and the mass of adsorbent (g).

The ion exchange experiment for mechanistic studies was conducted with the DTS in an excess amount of 0.02 M Cs^+ and Sr^{2+} solution, where V/m was equal to 500 mL/g. The mixture was stirred for 24 h at 25 °C. The ion exchanged material was washed several times with DI water, isolated by centrifugation before oven drying.

The individual Cs^+ and Sr^{2+} uptake were measured by adding 20 mg of the DTS into 20 mL of adsorbate solution at 25 °C. After 24 h of contact time, the adsorbent was separated from the liquid phase using a syringe filter (PTFE, 0.45 μm) and the residual adsorbate concentration in the filtrate was measured by ICP-MS. The obtained data were used to determine the adsorption isotherm.

The pH dependent performance study was carried out using three different solutions containing Cs^+, Sr^{2+} and a binary mixture of Cs^+ and Sr^{2+} (A^{n+}). The pH values were adjusted by adding HCl or NaOH into the prepared adsorbate solution ($C_{0,Cs}$ ~ 10 ppm, $C_{0,Sr}$ ~ 9 ppm). Ion exchange experiments under different Na^+ concentrations were also conducted by dissolving the required amount of NaCl in a solution containing Cs^+ and Sr^{2+} (C_0 ~ 1 ppm).

The removal kinetics of A^{n+} ions was evaluated under various reaction times from 1 min to 24 h. For each experiment, 20 mg of the DTS sample was added to 20 mL of a solution containing A^{n+} ions, and the mixture was shaken at 25 °C until the designated reaction time. The solution was then filtrated and the ion concentrations analyzed by ICP-MS.

Competitive ion exchange experiments were studied under various solution conditions. The individual ion effect for the DTS was evaluated in the presence of 0.05 M Na^+, K^+, Ca^{2+}, and Mg^{2+} ions. Comprehensive ionic effect for DTS was carried out in tap water, simulated groundwater and real seawater.

Continuous Cs^+ and Sr^{2+} separation experiments of GDM were conducted via vacuum filtration at room temperature. Typically, 20 mL of the wastewater was filtered each cycle through the fabricated membrane with an effective separation area of 11.3 cm^2, and the trans-membrane pressure was under 0.5 bar. The ionic concentrations of filtrate were then measured by ICP-MS.

Material Characterization

Field emission scanning electron microscopy (SEM) observation was conducted using a Hitachi SU8230. Transmission electron microscopy (TEM) was performed with a JEOL JEM-2100F (200 kV), and the elemental mapping image was obtained using a Titan cubed G2 60-300 (80 kV) coupled with an energy dispersive X-ray spectrometer (EDX). The samples for electron microscopy were dispersed in ethanol, followed by drop-wise casting on a 300 mesh copper grid. Powder x-ray diffraction (XRD) patterns were collected using Rigaku Smartlab with Cu Kα radiation (λ = 1.5406 Å) operated at 45 kV (200mA) and equipped with a high speed 1D detector (D/tex Ultra 250). Raman spectra of the samples were collected on ARAMIS (HORIBA) at a 514 nm Ar ion laser. X-ray photoelectron spectroscopy (XPS) data were obtained by K-alpha with a microfocused monochromatic Al Kα X-ray source (1486.6 eV). Samples were analyzed under an ultra-high vacuum condition of 10^{-9} Torr with a pass energy of 200 eV (survey scans) and 50 eV (high-resolution scans), and the peaks were referenced to the C1s peak (284.8 eV) of the surface adventitious carbon and fitted using the Avantage software. Atomic force microscopy (AFM) analysis of GO was performed with INNOVA-LABRAM HR800 (Horiba Jobin Yvon) using a tapping mode. The elemental composition was precisely measured by inductively coupled plasma optical emission spectrometer (ICP-OES, iCAP 6300 Duo, Thermo) by dissolving the titanosilicate in a hydrofluoric acid solution. The N_2 adsorption isotherm was measured using a Micromeritics 3Flex after degassing the sample under a high vacuum at 110 °C. The adsorbent zeta potentials were measured using a Zetasizer Nano ZSP (Malvern) as a function of the aqueous pH. Thermogravimetric analysis (TGA) was carried out using a TG209 F1 Libra (NETZSCH) under a N_2 flow at a heating rate of 10 °C/min.

Results & Discussion

Physicochemical analysis

To simplify the synthetic route and improve the simultaneous removal efficiency for Cs^+ and Sr^{2+}, the current study designed dual-cation incorporated pharmacosiderite type titanosilicate via a one-pot hydrothermal route (Fig. 1a), with $TiCl_3$ and sodium silicate

($Na_2O(SiO_2)_x$•xH_2O) used as Ti and Si precursors. After the hydrothermal treatment at 180 °C for 4 days a white precipitate had formed, which was analyzed by XRD and the spectra were compared to that of K^+ form of titanosilicate (K26L) that was developed earlier [34]. The XRD spectra for the two materials correspond to the simulated pattern of the pharmacosiderite titanosilicate (Figs. 1b and S1). For DTS, a shoulder and a split peak at around 28° and 38° indicated the presence of small amount of impurity. However, the elemental analyses obtained by ICP-OES were quite different between K26L and DTS. K26L had 14.4 wt% K, 12.1 wt% Si, and 22.2 wt% Ti, while DTS had 5.68 wt% K, 8.40 wt% Na, 12.0 wt% Si and 25.7 wt% Ti in the structure, revealing that the DTS contains dual cations of Na^+ and K^+ in the structure and larger amount of cations than K26L. With dual cations, the DTS represented the cubic nanocrystal structure as shown in TEM and SEM images (Figs. 1c and S2a). The fast Fourier transform (FFT) image additionally confirms a cubic structure of DTS along the [001] direction (Fig. 1d). Moreover, the elemental mapping results for Si, Ti, Na, and K support the homogeneous distribution of dual cations in the DTS structure (Fig. 1e). The presence of Si outside the focusing image (Si mapping result in Fig. 1e) suggests that the small amount of impurity was included in the synthesized DTS.

Ion exchange property of DTS

To identify the ion exchanged state of DTS, the specimen was immersed in a solution of 0.02 M Cs^+ and Sr^{2+}, respectively. The ion exchange process was continued for 24 h under stirring to ensure complete exchange. The XRD spectra of the exchanged materials retained their parent structure, showing the topotactic ion exchange process (Fig. 2a), with exchanged DTS remaining cubic-like as represented in the TEM and SEM images (Figs. 2b, c and Figs.

S2b, c). XRD peak shifting was noticeable in the DTS_Cs, indicating a change of the lattice distance by introducing the larger Cs^+ compared to the pre-occupied Na^+ and K^+ ions in the three-dimensional channel. Moreover, the ion dependent hydration of DTS was shown by TGA analyses (Fig. 2d), with DTS_Cs exhibiting the lowest level of hydration (6.7 wt%), and DTS_Sr having a higher degree of hydration (13.8 wt%), a result of Sr^{2+} being able to enter the channel in the partially hydrated form of $[Sr(H_2O)_x]^{2+}$ [1, 36].

The Raman spectra of the pristine, Cs^+ and Sr^{2+} exchanged DTS are presented in Fig. 2e. All materials showed strong bands at around 600 cm^{-1} and 930 cm^{-1}, which were assigned to the stretching of the Ti-O and Si-O bonds, respectively [34, 37]. The Ti-O associated peak of the Cs^+ exchanged DTS was significantly red-shifted to 580 cm^{-1} compared to the peak of the pristine material (602 cm^{-1}), reflecting the expansion of the TiO_6 octahedral units due to exchange with the larger radius Cs^+ [38]. Relatively, SiO_4 tetrahedral units were considered as being essentially rigid and hence a noticeable shift of the peak from 930 cm^{-1} was not observed [35, 39].

Direct observation of the XPS binding energy (BE) shift for the exchanged DTS is evidenced in Fig. 2f. The pristine DTS showed the characteristic $2p_{3/2}$ and $2p_{1/2}$ for Ti at 458.4 eV and 464.1 eV. The Ti2p peaks for the DTS_Sr shift to higher BE by 0.4 eV, which suggests that the local chemical state of Ti is influenced by the divalent Sr^{2+} incorporation into the cage of DTS [40]. Moreover, the Ti2p peak in the DTS_Cs XPS spectrum can be fitted as two peaks at 458.1 eV and 463.8 eV. The decrease in BE by 0.3 eV was attributed to the presence of the larger ionic radius Cs^+, thus Ti becomes a more electron-rich state. The change in the Na1s and K2p spectra following ion exchange with Cs^+ and Sr^{2+} will be discussed below.

Adsorption isotherm studies

In order to investigate the ion exchange capacity and affinity of DTS for Cs^+ and Sr^{2+}, the measured equilibrium data were evaluated using the well-known Langmuir and Langmuir-Freundlich adsorption isotherm models (Figs. 3a and b). The equilibrium constant and other related parameters are listed in Table 1.

Langmuir isotherm

$$Q = \frac{Q_m b C_e}{1 + bC_e} \qquad (4)$$

Langmuir-Freundlich isotherm

$$Q = \frac{Q_m (bC_e)^{1/n}}{1 + (bC_e)^{1/n}} \qquad (5)$$

where Q (mg/g) is the adsorbed amount of cations at the equilibrium concentration, and Q_m and b are the maximum adsorption capacity (mg/g) and the Langmuir affinity coefficient (L/mg), respectively. C_e is the equilibrium concentration (ppm) and n is a constant.

The Cs^+ equilibrium data was fitted using the Langmuir and Langmuir-Freundlich isotherms showing good agreement with $R^2 > 0.99$. The n value in the Langmuir-Freundlich model is 1.31, close to 1, indicating that Cs^+ adsorption follows the monolayer coverage of the Langmuir model. Considering the 8-membered cages of DTS, the pre-occupying Na^+ and K^+ cations can be exchanged with Cs^+, with the ions coordinated by framework oxygens. The Sr^{2+} equilibrium data was also fitted using both the Langmuir and Langmuir-Freundlich isotherms but shows different adsorption behaviors compared to Cs^+. The value of n in the Langmuir-Freundlich model is 2.53, much greater than 1, revealing that Sr^{2+} ion exchange deviates from the Langmuir model. This behavior can be understood when considering that the molar adsorption amount of Cs^+ (3.5 mmol/g) was 1.75 times higher than Sr^{2+} (2.0 mmol/g), hence Cs^+ ions have a higher amount of surface coverage, corresponding to a better Langmuir model fit [1]. Previous studies reported that the equilibrium adsorption behavior of the divalent cations tended to better follow the Langmuir-Freundlich isotherm than the Langmuir isotherm [1, 41].

The maximum adsorption capacities (Q_m) of Cs^+ and Sr^{2+} were found to be 469 mg/g and 179 mg/g, respectively. The obtained ion exchange capacities of DTS are compared with well-known Cs^+ or Sr^{2+} ion exchangers (Table 2), proving that the synthesized DTS has high adsorption capacities for the removal of these radionuclides. These capacities denote 69 % for Cs^+ and 80 % for Sr^{2+} of the theoretical ion exchange capacities (678 mg/g for Cs^+ and 223 mg/g for Sr^{2+}), based on the cation content in DTS. The higher charge normalized adsorption of Sr^{2+} (4.1 meq/g) than Cs^+ (3.5 meq/g) can be rationalized by the following three factors: (1) physical adsorption of the Sr^{2+} ions on the DTS surface due to the highly negative zeta potential ~ -40 mV (Fig. S3) [20], (2) formation of $Sr(OH)^+$ [42], and (3) precipitation of insoluble $Sr(OH)_2$ in the alkaline condition induced by the hydrolysis of DTS (the hydrolysis phenomena will be discussed below.) [30, 34].

To confirm the overestimation of Sr^{2+} adsorption capacity, XPS Na1s and K2p spectra for DTS, DTS_Cs and DTS_Sr were obtained following the ion exchange in an excess amount of 0.02 M Cs^+ and Sr^{2+} solution, respectively (Fig. 4). For each ion exchange, the prominent Cs^+ and Sr^{2+} related peaks were observed in the Cs3d (Fig. 4a) and Sr3d (Fig. 4b) spectra, respectively. The surface contents of Na^+ and K^+ for the exchanged DTS were significantly decreased compared to the XPS spectra of the pristine DTS. Regarding the Na1s spectra (Fig. 4c), both DTS_Cs and DTS_Sr indicate a similar intensity, but the K2p spectra (Fig. 4d) of DTS_Cs showed lower intensity than DTS_Sr. Thus, considering the ion exchange process between the cation in the structure and radionuclides to be removed, the DTS adsorbs more Cs^+ ions than Sr^{2+} ions.

The affinity for Cs^+ and Sr^{2+} ions was also evaluated in terms of the Langmuir constant b (L/mg) and distribution coefficient K_d (mL/g). A higher b value of 0.13 L/mg in Sr^{2+} indicated that DTS had a larger affinity for the divalent Sr^{2+} than the monovalent Cs^+ in the low concentration regime (Table 1) [1, 13]. In addition, to study the affinity in competing ionic solutions, K_d values were measured in the presence of both 10 ~ 50 ppm concentrated Cs^+ and Sr^{2+} (Fig. 5). In the case of 10 ppm, the K_d value for Sr^{2+} was higher than that of Cs^+, but as the concentration increased to 20 or 50 ppm, these two cations showed K_d values of a similar order of magnitude. Interestingly, even with coexistence of Cs^+ and Sr^{2+}, the K_d values of DTS were found to be higher than 10^4 mL/g (removal efficiency > 97 %) in all three cases of 10, 20 and 50 ppm, and a comparison of K_d values against other adsorbents including chalcogenide, titanosilicate, hexacyanoferrate and MOF (Table 2) revealed remarkable selectivity of Cs^+ and Sr^{2+} by DTS.

Ion exchange kinetics

To verify the kinetics of DTS purification of contaminated aqueous environments, ion exchange was performed in the presence of low concentration Cs^+ (~ 10 ppm) and Sr^{2+} (~ 9 ppm) solutions at 25 °C (Figs. 6a and b). The kinetics of individual ion adsorption (Fig. 6a) was exceptionally rapid and highly efficient, showing a removal efficiency of around 98 % for Cs^+ and greater than 99 % for Sr^{2+} within 1 min, with ultimate removal performances of 99.3 % and 99.7 % (K_d values of > 10^5 mL/g) for Cs^+ and Sr^{2+}, respectively. Moreover, DTS still exhibited fast kinetics even in a higher concentration of Cs^+ (~ 100 ppm) and Sr^{2+} (~ 75 ppm) solution with almost the same removal rate at contact times of 1 min and 24 h (Figs. 6c and d). To the best of our knowledge, DTS is one of the most effective ion exchangers in terms of removal kinetics. The layered metal sulfide, KTS-3 adsorbed 94 % and 92 % of the initial Cs^+ (~ 1.2 ppm) and Sr^{2+} (~ 1 ppm) ions within 5 min (V/m = 1000 mL/g), respectively [1]. FJSM-SnS exhibited fast equilibrium kinetics of 5 min at 65 °C, but it slowed to 30 min (Cs^+ ~ 128 ppm, V/m = 278 mL/g) and 60 min (Sr^{2+} ~ 44 ppm, V/m = 1000 mL/g) at a lower temperature of 17 °C [13].

The enhanced removal kinetics of DTS is partly related to the three-dimensional cubic structure. Moreover, the DTS crystallites form a mesoporous structure ranging from 10 to 40 nm, as indicated in the BJH desorption analysis (Fig. S4). The ionic solution can readily access active sites and thereby a rapid ion exchange process can occur. Even under binary conditions (Fig. 6b), DTS showed almost unaltered removal efficiencies as compared to the cases of individual ions, confirming once again the high adsorption capacity and the tremendous affinity of DTS for the simultaneous removal of Cs^+ and Sr^{2+}. The slight fluctuation observed in the kinetic curves reflects the dynamic ion exchange process, as observed by other inorganic ion exchangers [1, 13, 26]. For both individual and binary conditions, the adsorption kinetics follows a pseudo-second-order kinetic model implying that the rate of direct adsorption process controls the overall sorption kinetics (See Fig. S5) [43, 44].

pH stability

The pH of effluent is one of the most critical factors influencing the adsorption performance of radioactive cations, and hence removal rates were assessed across a wide pH range from 2 to 12 for individual and binary Cs^+ and Sr^{2+} solutions. Fig. 7a confirms that DTS exhibits excellent Cs^+ removal performance over the pH range. More than 99 % of Cs^+ ions were removed at pH 3 to 10. In highly acidic (pH 2) and basic (pH 12) conditions the Cs^+ removal performance was around 98 % and 96 %, respectively. In the case of Sr^{2+}, DTS exhibits remarkable removal performance with greater than 99 % at pH 3 to 12, but in strongly acidic conditions (pH 2) the removal efficiency drastically decreased to 24 %. Unlike Cs^+, the low capability for Sr^{2+} removal in pH 2 could be attributed to the formation of the protonated H-DTS. It was also reported that the protonated $H_4Ti_4O_4(SiO_4)_3\cdot 8H_2O$ showed negligible Sr^{2+} adsorption in acidic conditions [31], because it has a Ti-OH functional group that is less acidic than the Si-OH group in $H_2Ti_2O_3SiO_4\cdot 2H_2O$ (H-CST) [31, 33]. It is therefore more difficult to exchange with divalent Sr^{2+} ions in acidic conditions. For both Cs^+ and Sr^{2+}, the presence of competing ions (binary condition) is not detrimental to the adsorption performance because the DTS has rich ion exchange sites as demonstrated in the isotherm study.

To confirm the structural stability of DTS, XRD spectra were collected after 24 h contact time in various pH solutions (V/m = 1000 mL/g) at 25 °C under 200 rpm of shaking (Fig. 7b). At pH 2, the low intensity at around 11° and 23° suggests the formation of H-DTS [33], and the appearance of a sharp peak at 26° corresponds to TiO_2 due to slight decomposition of the DTS. However, in all other pH conditions, the stability of the DTS is very impressive. The ion exchanger retains its high crystalline structure even in a strongly basic environment (pH 12), and displays a very high simultaneous removal efficiency for Cs^+ and Sr^{2+}.

Removal selectivity

The distribution coefficients (K_d) and removal efficiencies for Cs^+ and Sr^{2+} are shown as a function of the Na^+ concentration (Fig. 8). The pure binary solution showed the highest K_d values for Cs^+ and Sr^{2+} due to the absence of competing Na^+. As the Na^+ concentration increased up to 0.25 M, the K_d value for Cs^+ and Sr^{2+} remained almost constant (slight increase). This increase can be described by the following equation:

$$M_3HTi_4O_4(SiO_4)\bullet 4H_2O + H_2O \Leftrightarrow M_{3-x}H_{1+x}Ti_4O_4(SiO_4)\bullet 4H_2O + xM^+ + xOH^- \ (M=Na^+ \text{ or } K^+) \quad (3)$$

As revealed by Eq (3), the hydrolysis reaction of DTS produces MOH, which increases the pH of the equilibrium solution [30, 34]. Increasing amounts of Na^+ in solution (0 ~ 1 M) lead to a shift to the left in the reaction scheme (3) and a decrease in the proportion of the hydrogen in the exchanger, as evidenced by a decrease of the equilibrium solution pH from 10.5 to 8.8. At higher Na^+ concentrations of 0.5 M and 1 M, the K_d values for these ions decrease due to the highly competitive effect of Na^+. However, even in the presence of 1 M Na^+, DTS still exhibits a high K_d of 2.2×10^4 mL/g for Cs^+ and 6.8×10^4 mL/g for Sr^{2+} along with high removal efficiencies of 95 % and 98 %. Such good performance demonstrates the material to be an effective adsorbent to treat dilute Cs^+ and Sr^{2+} solutions in concentrated Na^+ solutions.

To make our study more practical, DTS was tested in simulated groundwater, and real tap water and seawater conditions, in which Cs^+ and Sr^{2+} ions were diluted (Fig. 9a). From the contaminated groundwater and tap water systems, the K_d values were found to be more than 10^5 mL/g (% Removal > 99 %) for both Cs^+ and Sr^{2+}, demonstrating superior effectiveness of DTS for simultaneous removal of Cs^+ and Sr^{2+}. In the case of Sr^{2+}, the K_d values and removal efficiencies decreased in groundwater and especially seawater, compared to those of Cs^+. These performance degradations in Sr^{2+} relates to the presence of high concentration of divalent Ca^{2+} and Mg^{2+}, as can be speculated from the adsorption data against each competitive cation (Fig. 9b). However, even in seawater containing more than 10,000 times higher concentrated other cations, DTS still retains a high removal efficiency of 98 % and a high K_d of 4.9×10^4 mL/g for Cs^+. Thus, it can be concluded that the superior performance originates from the rich ion exchange sites, and the coexistence of K^+ and Na^+ in the structure enables DTS to have stable selectivity for Cs^+ and Sr^{2+} from the water system containing both K^+ and Na^+.

Continuous separation of Cs^+ and Sr^{2+} with graphene oxide (GO) and DTS composite membrane

From the viewpoint of process operation, the continuous separation of Cs^+ and Sr^{2+} using nanoparticles is difficult due to the filter clogging, pressure drop, and liquid / solid separation [15, 45, 46]. In order to mitigate these problems, GO was introduced to make a composite membrane with DTS. The used GO was synthesized with modified Hummer's method, and the results of characterization using Raman spectroscopy, XRD, and AFM are shown in Fig. S6. AFM image shows that the lateral size of each GO nanosheet appears to be less than 200 nm, and its thickness of 5-12 nm indicates the several layers of GO have been stacked (Figs. S6a and S6b) [47]. Previous studies have demonstrated that GO membrane had unique permeable properties to only H_2O molecules through narrow path between GO sheets [48, 49]. On the other hand, DTS has advantageous adsorption characteristics of very fast removal kinetics for both Cs^+ and Sr^{2+} with the formation of mesoporous cluster allowing the fast passage of ions (Fig. S4). Thus, in order to combine these two useful effects into one, the composite membrane (GDM) was synthesized by sequential steps of stacking GO thin layer on the bottom for proper liquid flux and placing DTS on it using a simple vacuum filtration method.

In order to elucidate a relation between the amount of GO and flux, different volumes of GO solutions were used in the preparation of the GO membranes. Regardless of the used volume of GO, all GO membranes exhibited distinct Raman peaks at around 1350 cm^{-1} and 1590 cm^{-1}, indicating that GO was successfully incorporated in the PES membrane (Fig. 10a) [50, 51]. The PES membrane indicated the highest flux of 1.5×10^4 $L{\cdot}m^2{\cdot}h^{-1}$, and the measured flux decreased with the increasing volume of used GO solutions (Fig. 10b). Among the prepared GO membranes, the GO20mL indicated a high flux of 1394 $L{\cdot}m^2{\cdot}h^{-1}$, which is much higher than flux of 512 $L{\cdot}m^{2}{\cdot}h^{-1}$ and 323 $L{\cdot}m^2{\cdot}h^{-1}$ from GO40mL and GO60mL.

The macroscopic image of GO20mL membrane indicated that the PES membrane was totally covered by GO, and DTS can be stably maintained on the GO20mL membrane (Fig. S7). Moreover, the SEM image of the PES membrane (Fig. 11a) showed the presence of around 0.2 μm sized pores on the structure, but the pores were covered by GO after vacuum filtration of 20 mL GO (Fig. 11b). The cross-sectional SEM image of GDM (Fig. 11c) represents that the DTS was supported by the preformed GO20mL membrane. Moreover, the EDX result along the indicated line in Fig. 10d showed two distinct layers, one of which was titanium and silica dominant layer corresponding to DTS, and the other of which was a PES layer having sulfur. Between the two layers, GO layer exists as indicated in Figs. S7 and 11b, but the carbon and oxygen originated from GO were not discriminated by the EDX because GO was embedded in the PES membrane as a very thin layer.

The removal performance of GDM was evaluated with an individual Cs^+ and Sr^{2+} solution (~ 5 ppm). GDM showed almost 100 % removal for both Cs^+ and Sr^{2+} implying the possible application of GDM for the continuous purification of the radionuclides (Fig. S8). Compared with the results from GDM, the pure GO membrane showed much lower removal rates of around 30 % (Fig. S8). This comparison clearly showed that the high performance is attributed to DTS rather than GO. In Fig. 12, the reusability of GDM was investigated by filtering 10 consecutive cycles of 20 mL of Cs^+ and Sr^{2+} binary tap water (C_0 ~ 1.7 ppm). The result exhibited that the membrane worked efficiently up to 10th cycles showing high removal efficiency above 98 ~ 99 % for 9 consecutive cycles and slight decrease of Sr^{2+} removal rate to 97 % at 10th cycle (Fig. 12a). In terms of stability, after immersion of the membrane in DI water for 24 h, the recovered GDM maintained excellent result (Fig. 12b) similar to that in the pristine GDM before immersion (Fig. 12a).

To be making the prepared GDM more practical, the simulant groundwater (C_0 ~ 1 ppm) was also used as feed solution for 10 cycles (Fig. 12c). The increase in the concentration of filtrate Cs^+ and Sr^{2+} from 0.57 ppb to 35.80 ppb and 5.43 ppb to 100.08 ppb, respectively, over the 10 cycles is possibly related to a slight saturation of DTS in GDM and competitive effect by Na^+, K^+, Ca^{2+}, and Mg^{2+}, but GDM still showed around 90 % of removal efficiency for both Cs^+ and Sr^{2+} during 10 cycles. It is worth highlighting that around 90 % of 200 mL groundwater contaminated with Cs^+ and Sr^{2+} (20 mL × 10 cycles) was continuously purified using only 0.04 g of DTS. Finally, GDM was tested in seawater containing ~ 1 ppm of Cs^+ (6.5 ppm of Sr^{2+} already dissolved in seawater). It retained above 90 % Cs^+ removal efficiency up to 5 cycles and indicated 71 % of Cs^+ removal at 10th cycle even in the presence of highly competitive seawater condition (Fig. 12d), though Sr^{2+} was difficult to be removed due to the interference of highly concentrated divalent ions of Ca^{2+} and Mg^{2+} as shown in Fig. 9. Thus, the synthesized GDM shed the light on the application of DTS as continuous process based on extremely fast adsorption kinetics and large capacity.

Conclusions

This study has demonstrated the application of the dual-cation form of pharmacosiderite type titanosilicate as an efficient ion-exchanger for the simultaneous removal of Cs^+ and Sr^{2+}. The dual cations of Na^+ and K^+ are incorporated into the three-dimensional cubic structure interconnected by silicate and titanium and ion exchange with Cs^+ and Sr^{2+}. It is remarkable that DTS showed high capacity and rapid removal kinetics with a broad pH resistance. DTS exhibited superior selectivity for both diluted Cs^+ and Sr^{2+} as high as more than 10^5 mL/g of K_d values in contaminated tap water and groundwater, and a greatly promising Cs^+ selectivity of 4.9×10^4 mL/g even in seawater. The high-performance retention in complex ionic solutions relates to the dual-cation incorporation, leading to continuous affinity for Cs^+ and Sr^{2+} in the presence of a large amount of K^+ as well as Na^+. In the practical point of view, DTS was utilized as the composite membrane with GO for continuous separation of Cs^+ and Sr^{2+}, and the process showed promising high removal efficiencies during 10 consecutive cycles in tap water, groundwater and seawater. Considering the simple and economic one-step synthesis route, this study demonstrates the practicality of the dual-cation incorporated DTS to treat radionuclide contaminated effluents.

References

[1] D. Sarma, C.D. Malliakas, K.S. Subrahmanyam, S.M. Islama, M.G. Kanatzidis, K2xSn4-xS8-x (x=0.65-1): a new metal sulfide for rapid and selective removal of Cs+, Sr2+ and UO22+ ions, Chemical Science, 7 (2016) 1121-1132.

[2] H.J. Yang, H.Y. Li, J.L. Zhai, L. Sun, Y. Zhao, H.W. Yu, Magnetic prussian blue/graphene oxide nanocomposites caged in calcium alginate microbeads for elimination of cesium ions from water and soil, Chemical Engineering Journal, 246 (2014) 10-19.

[3] S.J. Datta, W.K. Moon, D.Y. Choi, I.C. Hwang, K.B. Yoon, A Novel Vanadosilicate with Hexadeca-Coordinated Cs+ Ions as a Highly Effective Cs+ Remover, Angewandte Chemie-International Edition, 53 (2014) 7203-7208.

[4] Y. Kim, I. Kim, T.S. Lee, E. Lee, K.J. Lee, Porous hydrogel containing Prussian blue nanoparticles for effective cesium ion adsorption in aqueous media, Journal of Industrial and Engineering Chemistry, 60 (2018) 465-474.

[5] T.Y. Kim, S.S. An, W.G. Shim, J.W. Lee, S.Y. Cho, J.H. Kim, Adsorption and energetic heterogeneity properties of cesium ions on ion exchange resin, Journal of Industrial and Engineering Chemistry, 27 (2015) 260-267.

[6] Y.K. Kim, Y. Kim, S. Kim, D. Harbottle, J.W. Lee, Solvent-assisted synthesis of potassium copper hexacyanoferrate embedded 3D-interconnected porous hydrogel for highly selective and rapid cesium ion removal, Journal of Environmental Chemical Engineering, 5 (2017) 975-986.

[7] A.A. Kadam, J. Jang, D.S. Lee, Facile synthesis of pectin-stabilized magnetic graphene oxide Prussian blue nanocomposites for selective cesium removal from aqueous solution, Bioresource Technology, 216 (2016) 391-398.

[8] J.Y. Yoon, H. Zhang, Y.K. Kim, D. Harbottle, J.W. Lee, A high-strength polyvinyl alcohol hydrogel

membrane crosslinked by sulfosuccinic acid for strontium removal via filtration, Journal of Environmental Chemical Engineering, 7 (2019) 102824.

[9] N. Yoshida, J. Kanda, Tracking the Fukushima Radionuclides, Science, 336 (2012) 1115-1116.

[10] A. Clearfield, D.G. Medvedev, S. Kerlegon, T. Bosser, J.D. Burns, M. Jackson, Rates of Exchange of Cs+ and Sr2+ for Poorly Crystalline Sodium Titanium Silicate (CST) in Nuclear Waste Systems, Solvent Extraction and Ion Exchange, 30 (2012) 229-243.

[11] C.C. Pavel, K. Popa, Investigations on the ion exchange process of Cs+ and Sr2+ cations by ETS materials, Chemical Engineering Journal, 245 (2014) 288-294.

[12] S. Baik, H. Zhang, Y.K. Kim, D. Harbottle, J.W. Lee, Enhanced adsorption capacity and selectivity towards strontium ions in aqueous systems by sulfonation of CO2 derived porous carbon, RSC Advances, 7 (2017) 54546-54553.

[13] X.-H. Qi, K.-Z. Du, M.-L. Feng, J.-R. Li, C.-F. Du, B. Zhang, X.-Y. Huang, A two-dimensionally microporous thiostannate with superior Cs+ and Sr2+ ion-exchange property, Journal of Materials Chemistry A, 3 (2015) 5665-5673.

[14] R. Turgis, G. Arrachart, C. Delchet, C. Rey, Y. Barre, S. Pellet-Rostaing, Y. Guari, J. Larionova, A. Grandjean, An Original "Click and Bind" Approach for Immobilizing Copper Hexacyanoferrate Nanoparticles on Mesoporous Silica, Chemistry of Materials, 25 (2013) 4447-4453.

[15] Y.K. Kim, T. Kim, Y. Kim, D. Harbottle, J.W. Lee, Highly effective Cs+ removal by turbidity-free potassium copper hexacyanoferrate-immobilized magnetic hydrogels, J Hazard Mater, 340 (2017) 130-139.

[16] A. Nilchi, R. Saberi, M. Moradi, H. Azizpour, R. Zarghami, Adsorption of cesium on copper hexacyanoferrate-PAN composite ion exchanger from aqueous solution, Chemical Engineering Journal, 172 (2011) 572-580.

[17] Y. Kim, Y.K. Kim, S. Kim, D. Harbottle, J.W. Lee, Nanostructured potassium copper hexacyanoferrate-cellulose hydrogel for selective and rapid cesium adsorption, Chemical Engineering Journal, 313 (2017) 1042-1050.

[18] B. Aguila, D. Banerjee, Z. Nie, Y. Shin, S. Ma, P.K. Thallapally, Selective removal of cesium and strontium using porous frameworks from high level nuclear waste, Chemical Communications, 52 (2016) 5940-5942.

[19] J. Jang, D.S. Lee, Enhanced adsorption of cesium on PVA-alginate encapsulated Prussian blue-graphene oxide hydrogel beads in a fixed-bed column system, Bioresource Technology, 218 (2016) 294-300.

[20] N. Li, L. Zhang, Y. Chen, M. Fang, J. Zhang, H. Wang, Highly efficient, irreversible and selective ion exchange property of layered titanate nanostructures, Advanced Functional Materials, 22 (2012) 835-841.

[21] K. Wang, H. Ma, S. Pu, C. Yan, M. Wang, J. Yu, X. Wang, W. Chu, A. Zinchenko, Hybrid porous magnetic bentonite-chitosan beads for selective removal of radioactive cesium in water, Journal of Hazardous Materials, 362 (2019) 160-169.

[22] S.B. Yang, C. Han, X.K. Wang, M. Nagatsu, Characteristics of cesium ion sorption from aqueous

solution on bentonite- and carbon nanotube-based composites, J Hazard Mater, 274 (2014) 46-52.

[23] H.L. Chang, W.H. Shih, A general method for the conversion of fly ash into zeolites as ion exchangers for cesium, Industrial & Engineering Chemistry Research, 37 (1998) 71-78.

[24] Y. Kim, Y.K. Kim, J.H. Kim, M.-S. Yim, D. Harbottle, J.W. Lee, Synthesis of functionalized porous montmorillonite via solid-state NaOH treatment for efficient removal of cesium and strontium ions, Applied Surface Science, 450 (2018) 404-412.

[25] H. Zhang, S. Tangparitkul, B. Hendry, J. Harper, Y.K. Kim, T.N. Hunter, J.W. Lee, D. Harbottle, Selective separation of cesium contaminated clays from pristine clays by flotation, Chemical Engineering Journal, 355 (2019) 797-804.

[26] H. Yang, M. Luo, L. Luo, H. Wang, D. Hu, J. Lin, X. Wang, Y. Wang, S. Wang, X. Bu, P. Feng, T. Wu, Highly Selective and Rapid Uptake of Radionuclide Cesium Based on Robust Zeolitic Chalcogenide via Stepwise Ion-Exchange Strategy, Chemistry of Materials, 28 (2016) 8774-8780.

[27] A. Clearfield, Inorganic Ion Exchangers: A Technology Ripe for Development, Industrial & Engineering Chemistry Research, 34 (1995) 2865-2872.

[28] L. Al-Attar, A. Dyer, A. Paajanen, R. Harjula, Purification of nuclear wastes by novel inorganic ion exchangers, Journal of Materials Chemistry, 13 (2003) 2969-2974.

[29] H.M. Liu, A. Yonezawa, K. Kumagai, M. Sano, T. Miyake, Cs and Sr removal over highly effective adsorbents ETS-1 and ETS-2, Journal of Materials Chemistry A, 3 (2015) 1562-1568.

[30] A. Dyer, M. Pillinger, S. Amin, Ion exchange of caesium and strontium on a titanosilicate analogue of the mineral pharmacosiderite, Journal of Materials Chemistry, 9 (1999) 2481-2487.

[31] A.M. Puziy, Cesium and strontium exchange by the framework potassium titanium silicate K3HTi4O4(SiO4)3·4H2O, Journal of Radioanalytical and Nuclear Chemistry, 237 (1998) 73-80.

[32] D.M. Chapman, A.L. Roe, Synthesis, characterization and crystal chemistry of microporous titanium-silicate materials, Zeolites, 10 (1990) 730-737.

[33] E.A. Behrens, D.M. Poojary, A. Clearfield, Syntheses, Crystal Structures, and Ion-Exchange Properties of Porous Titanosilicates, HM3Ti4O4(SiO4)3·4H2O (M = H+, K+, Cs+), Structural Analogues of the Mineral Pharmacosiderite, Chemistry of Materials, 8 (1996) 1236-1244.

[34] E.A. Behrens, A. Clearfield, Titanium silicates, M3HTi4O4(SiO4)3·4H2O (M=Na+, K+),with three-dimensional tunnel structures for the selective removal of strontium and cesium from wastewater solutions, Microporous Materials, 11 (1997) 65-75.

[35] M.S. Dadachov, W.T.A. Harrison, Synthesis and Crystal Structure of Na4[(TiO)4(SiO4)3]·6H2O, a Rhombohedrally Distorted Sodium Titanium Silicate Pharmacosiderite Analogue, Journal of Solid State Chemistry, 134 (1997) 409-415.

[36] J.L. Mertz, Z.H. Fard, C.D. Malliakas, M.J. Manos, M.G. Kanatzidis, Selective Removal of Cs+, Sr2+, and Ni2+ by K2xMgxSn3-xS6 (x=0.5-1) (KMS-2) Relevant to Nuclear Waste Remediation, Chemistry of Materials, 25 (2013) 2116-2127.

[37] C. Li, G. Xiong, J. Liu, P. Ying, Q. Xin, Z. Feng, Identifying framework titanium in TS-1 zeolite by UV resonance Raman spectroscopy, The Journal of Physical Chemistry B, 105 (2001) 2993-2997.

[38] M. Giese, L.K. Blusch, M.K. Khan, M.J. MacLachlan, Functional Materials from Cellulose-Derived

Liquid-Crystal Templates, Angewandte Chemie International Edition, 54 (2015) 2888-2910.

[39] M.A. Roberts, A.N. Fitch, A.V. Chadwick, The crystal structures of (NH4)3HGe7O16·nH2O and Li4−xHxGe7O16·nH2O determined from powder diffraction data using synchrotron radiation, Journal of Physics and Chemistry of Solids, 56 (1995) 1353-1358.

[40] J. Zhu, Z. Deng, F. Chen, J. Zhang, H. Chen, M. Anpo, J. Huang, L. Zhang, Hydrothermal doping method for preparation of Cr3+-TiO2 photocatalysts with concentration gradient distribution of Cr3+, Applied Catalysis B: Environmental, 62 (2006) 329-335.

[41] D. Sarma, S.M. Islam, K. Subrahmanyam, M.G. Kanatzidis, Efficient and selective heavy metal sequestration from water by using layered sulfide K 2x Sn 4− x S 8− x (x= 0.65–1; KTS-3), Journal of Materials Chemistry A, 4 (2016) 16597-16605.

[42] J. Lehto, A. Clearfield, The ion exchange of strontium on sodium titanate Na4Ti9O20. xH2O, Journal of radioanalytical and nuclear chemistry, 118 (1987) 1-13.

[43] W. Plazinski, W. Rudzinski, A. Plazinska, Theoretical models of sorption kinetics including a surface reaction mechanism: A review, Advances in Colloid and Interface Science, 152 (2009) 2-13.

[44] I.M. Ali, E.S. Zakaria, H.F. Aly, Highly effective removal of 22Na, 134Cs and 60Co from aqueous solutions by titanosilicate: a radiotracer study, Journal of Radioanalytical and Nuclear Chemistry, 285 (2010) 483-489.

[45] Y.K. Kim, K. Bae, Y. Kim, D. Harbottle, J.W. Lee, Immobilization of potassium copper hexacyanoferrate in doubly crosslinked magnetic polymer bead for highly effective Cs+ removal and facile recovery, Journal of Industrial and Engineering Chemistry, (2018).

[46] H. Roh, Y. Kim, Y.K. Kim, D. Harbottle, J.W. Lee, Amino-functionalized magnetic chitosan beads to enhance immobilization of potassium copper hexacyanoferrate for selective Cs+ removal and facile recovery, RSC Advances, 9 (2019) 1106-1114.

[47] J. Zhang, Y. Zhao, X. Guan, R.E. Stark, D.L. Akins, J.W. Lee, Formation of Graphene Oxide Nanocomposites from Carbon Dioxide Using Ammonia Borane, The Journal of Physical Chemistry C, 116 (2012) 2639-2644.

[48] R.R. Nair, H.A. Wu, P.N. Jayaram, I.V. Grigorieva, A.K. Geim, Unimpeded Permeation of Water Through Helium-Leak-Tight Graphene-Based Membranes, Science, 335 (2012) 442-444.

[49] J. Abraham, K.S. Vasu, C.D. Williams, K. Gopinadhan, Y. Su, C.T. Cherian, J. Dix, E. Prestat, S.J. Haigh, I.V. Grigorieva, P. Carbone, A.K. Geim, R.R. Nair, Tunable sieving of ions using graphene oxide membranes, Nat Nanotechnol, 12 (2017) 546-+.

[50] C. Meng, Q. Chen, X. Li, H. Liu, Controlling covalent functionalization of graphene oxide membranes to improve enantioseparation performances, Journal of Membrane Science, 582 (2019) 83-90.

[51] F. Zhou, H.N. Tien, Q. Dong, W.L. Xu, H. Li, S. Li, M. Yu, Ultrathin, ethylenediamine-functionalized graphene oxide membranes on hollow fibers for CO2 capture, Journal of Membrane Science, 573 (2019) 184-191.

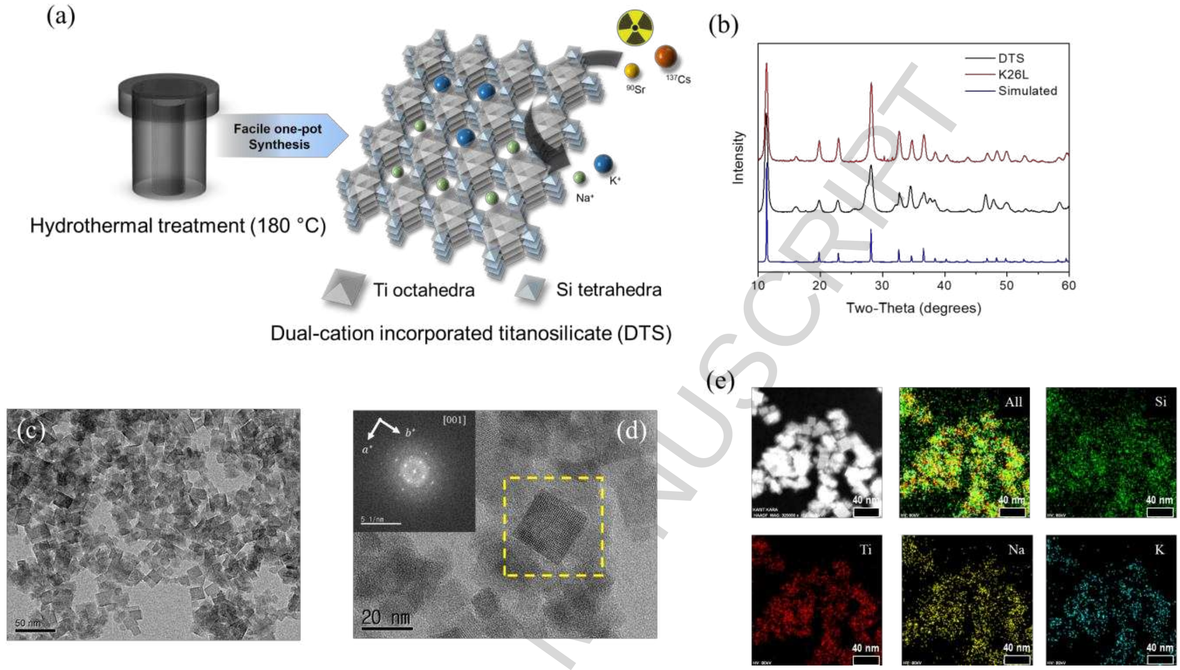

Fig. 1. (a) Schematic representation for synthesis of DTS, and cesium and strontium removal. (b) XRD patterns for DTS, K26L and simulated pharmacosiderite type titanosilicate ($K_3HTi_4O_4(SiO_4)_3 \cdot 4H_2O$). (c) TEM and (d) high resolution TEM images with the corresponding FFT image (inset) of DTS. (e) Elemental mapping results for DTS.

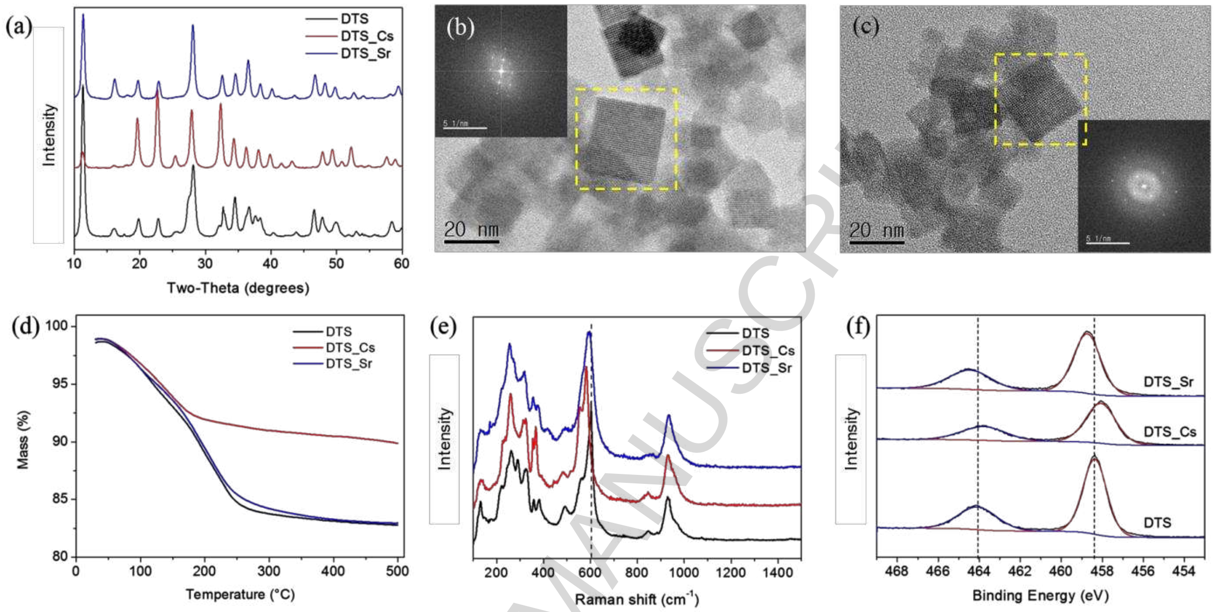

Fig. 2. (a) XRD patterns for pristine DTS, Cs^+ exchanged DTS (DTS_Cs) and Sr^{2+} exchanged DTS (DTS_Sr). High resolution TEM images of (b) DTS_Cs and (c) DTS_Sr with the corresponding FFT image (inset). (d) TGA profile, (e) Raman spectra, and (f) XPS Ti2p spectra for pristine DTS, DTS_Cs and DTS_Sr.

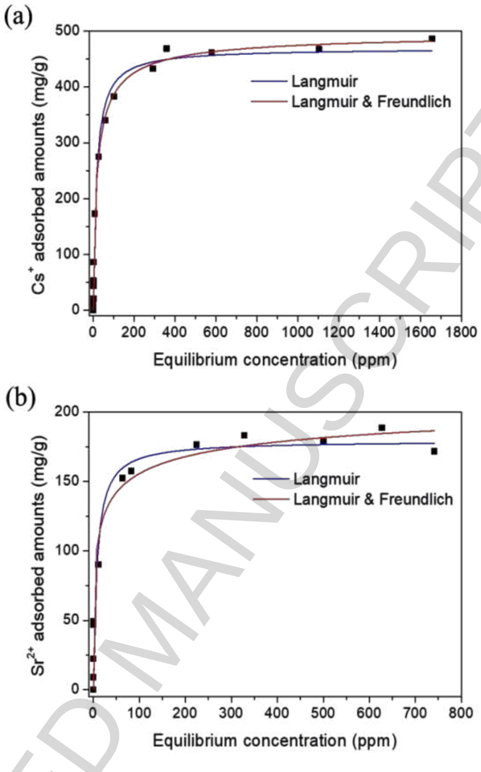

Fig. 3. Adsorption isotherms at 25 °C for (a) Cs$^+$ and (b) Sr^{2+} with Langmuir and Langmuir-Freundlich fitting curves (V/m was set to

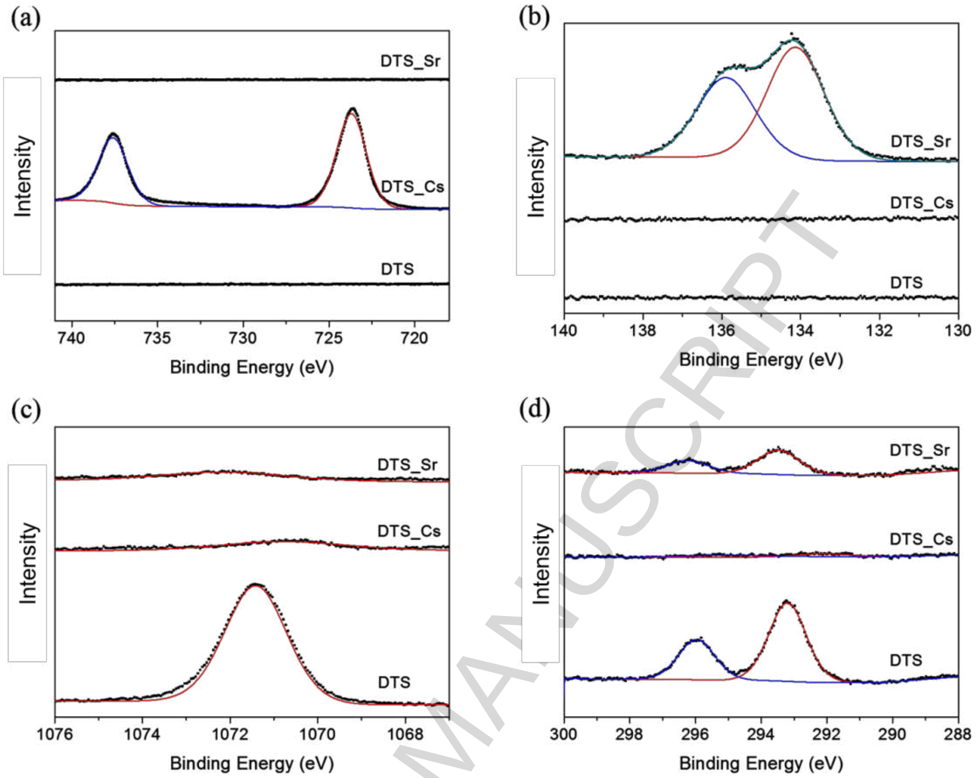

Fig. 4. XPS (a) Cs3d, (b) Sr3d, (c) Na1s, and (d) K2p spectra for DTS, DTS_Cs and DTS_Sr.

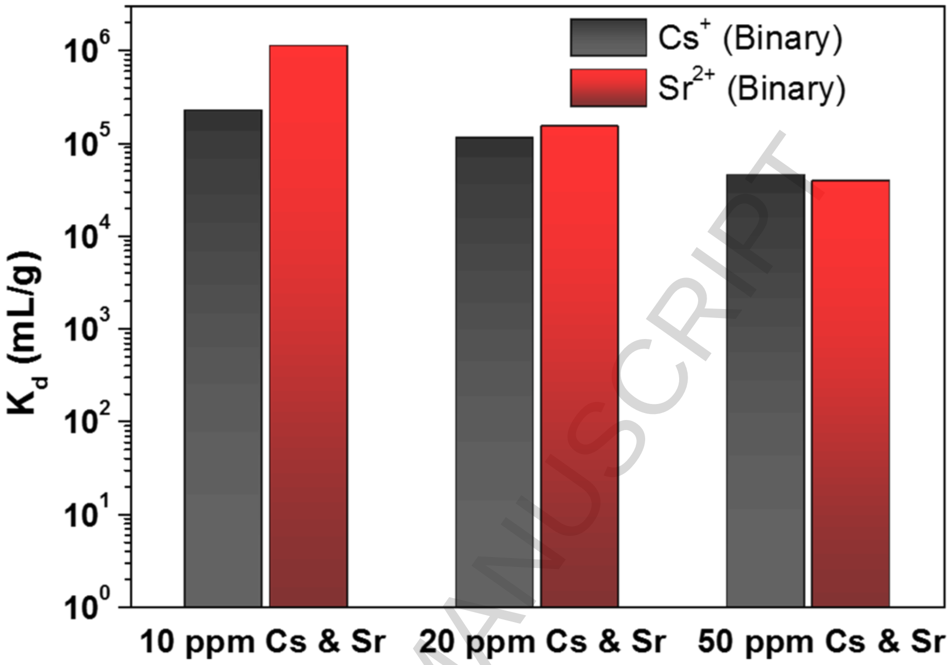

Fig. 5. Distribution coefficient for Cs$^+$ and Sr^{2+} in binary conditions.

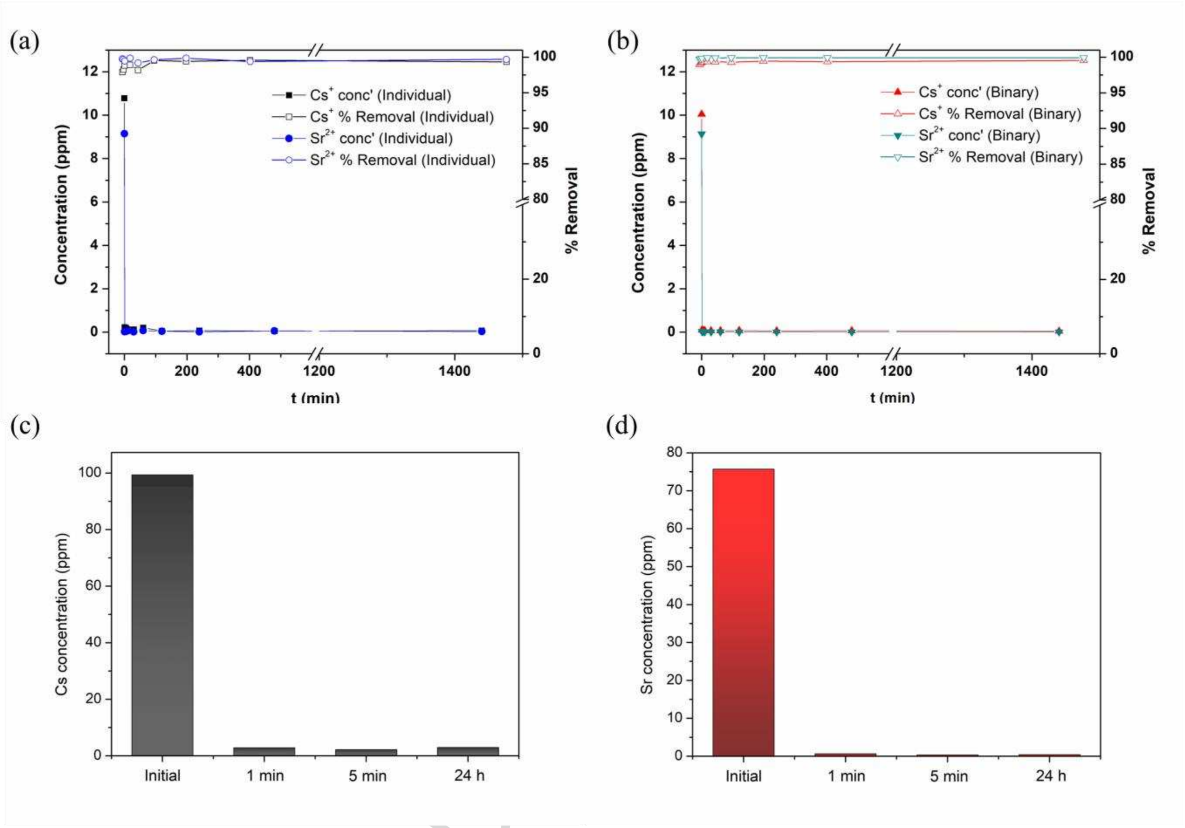

Fig. 6. Removal kinetics for (a) individual and (b) binary Cs^+ (~ 10 ppm) and Sr^{2+} (~ 9 ppm). Residual concentration of (c) Cs^+ (~ 100 ppm) and (d) Sr^{2+} (~ 75 ppm) over adsorption time.

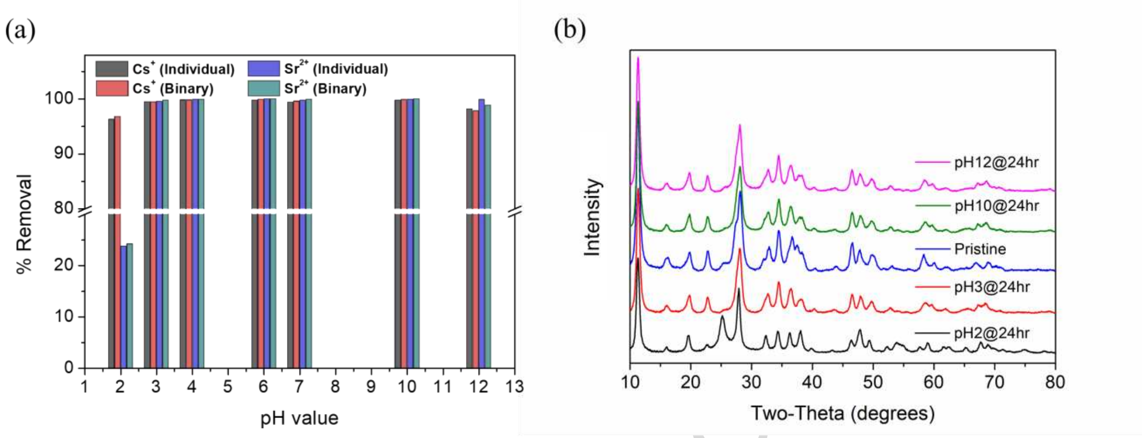

Fig. 7. (a) pH-dependent Cs^+ and Sr^{2+} uptake in individual and binary conditions. Initial concentrations of Cs^+ and Sr^{2+} were set to around 10 ppm and 9 ppm, respectively. (b) pH-dependent XRD patterns for DTS. The mixture was shaken for 24 h at 25 °C (V/m was set to be 1000 mL/g).

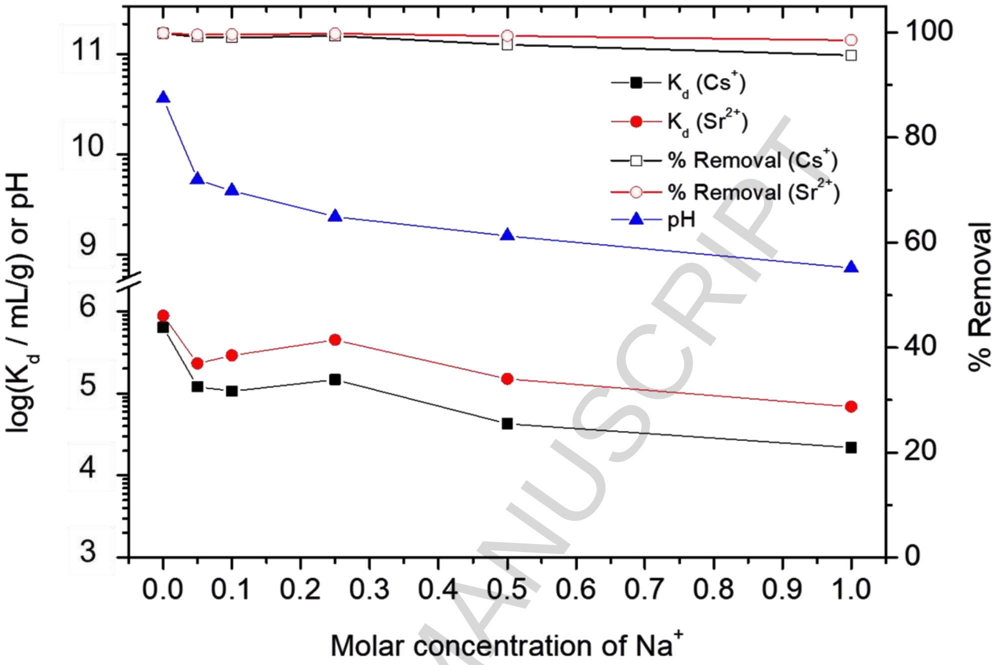

Fig. 8. Variation of distribution coefficient and removal rate of Cs^+ and Sr^{2+}, and the corresponding equilibrium pH with increasing molar concentration of Na^+. The initial concentrations of Cs^+ and Sr^{2+} were set to around 1ppm.

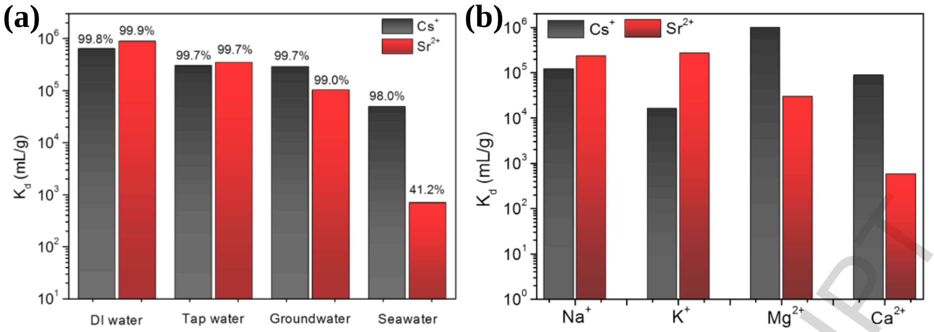

Fig. 9. (a) Cs^+ and Sr^{2+} distribution coefficient in tap water, simulated groundwater and seawater conditions. In tap water (16 ppm Na^+, 4.6 ppm K^+, 5 ppm Mg^{2+}, 12 ppm Ca^{2+}) and groundwater (115 ppm Na^+, 181 ppm K^+, 112 ppm Mg^{2+}, 25 ppm Ca^{2+}), the initial concentration of Cs^+ and Sr^{2+} were set to around 1 ppm. In seawater (9702 ppm Na^+, 321 ppm K^+, 1085 ppm Mg^{2+}, 99 ppm Ca^{2+}, 7.1 ppm Sr^{2+}), the initial concentration of Cs^+ was set to be around 1 ppm. (b) Distribution coefficient of Cs^+ and Sr^{2+} (binary) in the presence of 0.05 M competing cations. The initial concentrations of both Cs^+ and Sr^{2+} were set to be around 1 ppm.

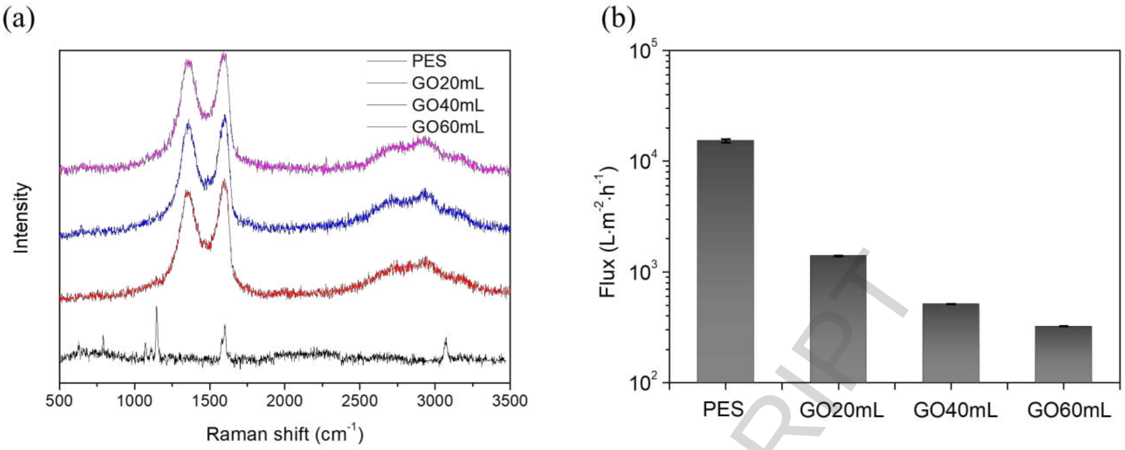

Fig. 10. (a) Raman spectra and (b) water flux for PES, GO20mL, GO40mL and GO60mL membranes.

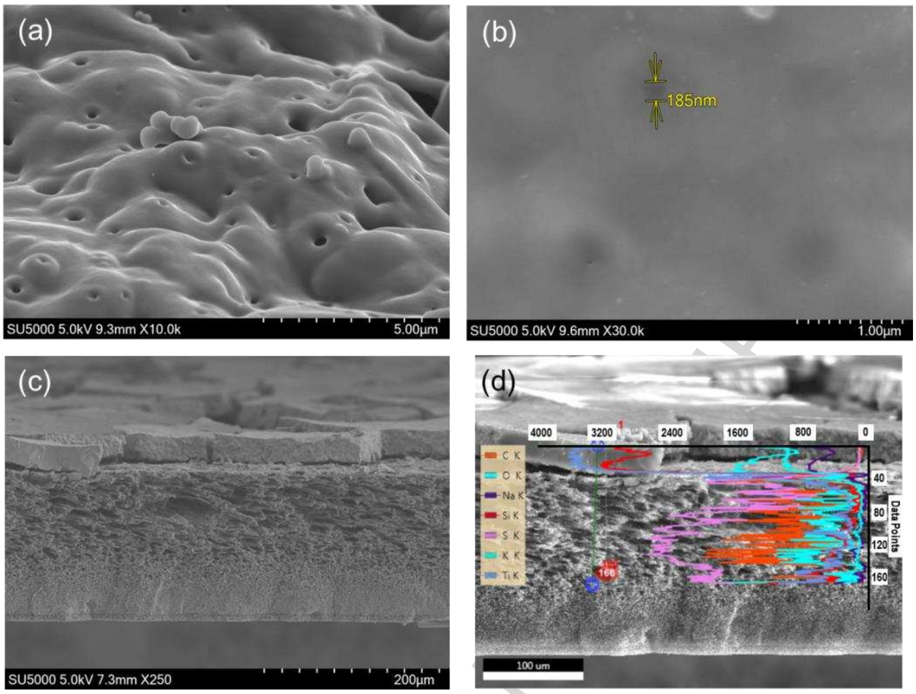

Fig. 11. SEM images of (a) PES and (b) GO20mL membranes. Cross-sectional SEM image of (c) GDM and (d) EDS result according to cross-sectional surface of GDM.

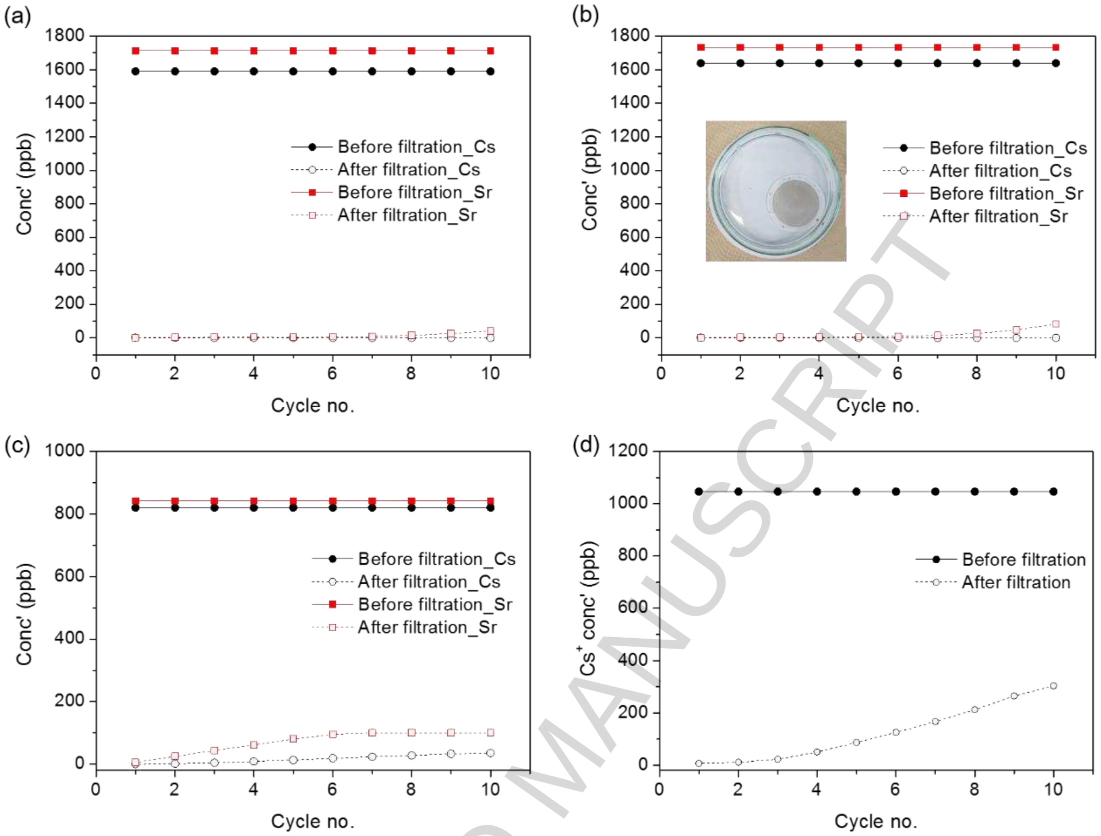

Fig. 12. 10 cycles of filtration results in tap water (a) before and (b) after immersion of GDM in DI water for 24 h, and in (c) simulated groundwater and (d) real seawater with pristine GDM.

Table 1 Fitting parameter for Cs^+ and Sr^{2+} equilibrium data obtained with Langmuir and Langmuir-Freundlich models.

	Langmuir			Langmuir-Freundlich			
	b (L/mg)	q_m (mg/g)	R^2	b (L/mg)	q_m (mg/g)	n	R^2
Cs^+	0.063	469	0.99	0.051	499	1.31	0.99
Sr^{2+}	0.13	179	0.93	0.082	223	2.53	0.97

Table 2 Comparison of Cs^+ and Sr^{2+} adsorption capacity and distribution coefficient for various adsorbents.

	$Q_{m,Cs}$* (mg/g)	$Q_{m,Sr}$* (mg/g)	$K_{d,Cs}$ (mL/g)	$K_{d,Sr}$ (mL/g)	Adsorption condition**	Reference
KMS-2	532	87	7.1×10^3	2.1×10^4	$C_{0,Cs}$ & $C_{0,Sr}$ (binary) ~6 ppm, V/m=1000 mL/g at RT	[36]
KTS-3	280	102	5.5×10^4	3.9×10^5	$C_{0,Cs}$ & $C_{0,Sr}$(binary) ~6-8 ppm, V/m=1000 mL/g at RT	[1]
FJSM-SnS	409	65	$\sim3.0\times10^4$	$\sim9.0\times10^4$	$C_{0,Cs}$ ~5-8 ppm, $C_{0,Sr}$ ~2-7 ppm, V/m=1000 mL/g at 65 °C	[13]
K@RWY	310	-	$\geq 10^5$	-	$C_{0,Cs}$ ~10 ppm, V/m=1000 mL/g at RT	[26]
HCF-gel-4	308	-	1.6×10^5	-	$C_{0,Cs}$ ~9 ppm, V/m=2000 mL/g at 25 °C	[17]
MIL-101-SO_3H	453	-	- (RE: 99.99 %)	$\sim2.3\times10^4$	$C_{0,Cs}$ ~145 ppm, $C_{0,Sr}$ ~82 ppm, V/m=250 mL/g	[18]
ETS-4	~797	~219	-	-	-	[11]
Na26L & K26L	415	105	-	-	-	[34]
ETS-1 1d & ETS-2 1d	346	159	-	-	-	[29]
DTS	469	179	2.2×10^5	1.1×10^6	$C_{0,Cs}$ & $C_{0,Sr}$ (binary) ~10 ppm, V/m=1000 mL/g at 25 ℃	This work

* Saturation capacity for Cs and Sr

** $K_{d,Cs}$ and $K_{d,Sr}$ are calculated by using the adsorption condition

Graphical Abstract

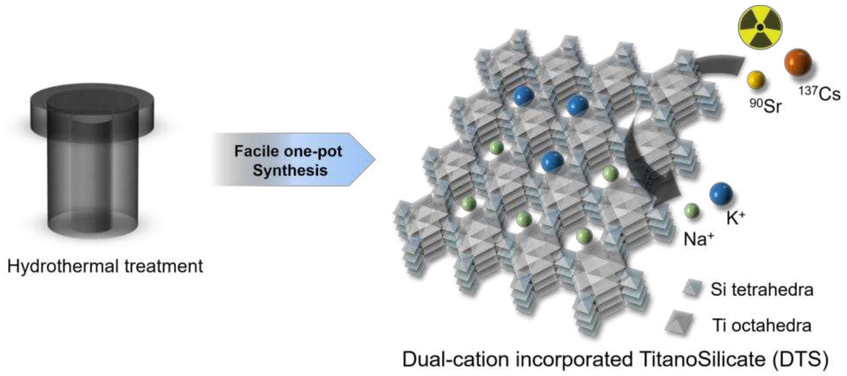

Facile one-pot synthesis of dual-cation incorporated titanosilicate and its deposition to membrane surfaces for simultaneous removal of Cs^+ and Sr^{2+}

Yun Kon Kim[a], Sungjun Kim[a], Yonghwan Kim[a], Kyeonghui Bae[a], David Harbottle[b] and Jae W. Lee [a],*

[a]Department of Chemical and Biomolecular Engineering, Korea Advanced Institute of Science and Technology (KAIST), Daejeon 305-701, Republic of Korea

[b]School of Chemical and Process Engineering, University of Leeds, Leeds LS2 9JT, United Kingdom

*Corresponding author. Tel: +82-42-350-3940. E-mail: jaewlee@kaist.ac.kr

KEYWORDS: Cesium, Strontium, Titanosilicate, Ion exchange, Membrane

Highlights

- Dual-cation form of DTS was synthesized via a facile one-pot hydrothermal route.
- DTS showed superior Cs^+ and Sr^{2+} adsorption capacities with very fast kinetics.
- Even in real-water systems, DTS exhibited high selectivity for Cs^+ and Sr^{2+}.
- DTS was used as a membrane with GO for continuous separation of Cs^+ and Sr^{2+}.